Title

13C NMR Metabolomic Evaluation of Immediate and Delayed Mild Hypothermia in Cerebrocortical Slices after Oxygen–Glucose Deprivation

Journal

Anesthesiology, 119(5)

ISSN

0003-3022

Authors

Liu, Jia
Segal, Mark R
Kelly, Mark JS
et al.

Publication Date

2013-11-01

DOI

10.1097/aln.0b013e31829c2d90

Peer reviewed

Published in final edited form as:
Anesthesiology. 2013 November ; 119(5): 1120–1136. doi:10.1097/ALN.0b013e31829c2d90.

^{13}C NMR Metabolomic Evaluation of Immediate and Delayed Mild Hypothermia in Cerebrocortical Slices After Oxygen-Glucose Deprivation

Jia Liu, M.D.[*], **Mark Segal, Ph.D.**[†], **Mark J.S. Kelly, Ph.D.**[‡], **Jeffrey G. Pelton, Ph.D.**[§], **Myungwon Kim, M.D.**[||], **Thomas L. James, Ph.D.**[#], and **Lawrence Litt, Ph.D., M.D.**[**]

[*]Research Associate, The Department of Anesthesia and Perioperative Care, The University of California San Francisco

[||]Visiting Professor, The Department of Anesthesia and Perioperative Care, The University of California San Francisco

[**]Professor, The Department of Anesthesia and Perioperative Care, The University of California San Francisco

[†]Professor, The Department of Epidemiology and Biostatistics, The University of California San Francisco

[‡]Research Associate Professor, The Department of Pharmaceutical Chemistry, The University of California San Francisco

[#]Professor, The Department of Pharmaceutical Chemistry, The University of California San Francisco

[§]NMR Spectroscopist and Laboratory Manager, QB3 Physical Biosciences Division, Lawrence Berkeley National Laboratory, The University of California, Berkeley

Abstract

Background—Mild brain hypothermia (32°C–34°C) after human neonatal asphyxia improves neurodevelopmental outcomes. Astrocytes but not neurons have pyruvate carboxylase (PC) and an acetate uptake transporter. ^{13}C NMR spectroscopy of rodent brain extracts after administering [1-^{13}C]glucose and [1,2-^{13}C]acetate can distinguish metabolic differences between glia and neurons, and tricarboxylic acid cycle (TCA cycle) entry *via* pyruvate dehydrogenase (PDH) and PC.

Methods—Neonatal rat cerebrocortical slices receiving a ^{13}C-acetate/glucose mixture underwent a 45-min asphyxia simulation *via* oxygen-glucose-deprivation (OGD) followed by 6 h of recovery. Protocols in three groups of N = 3 experiments were identical except for temperature management. The three temperature groups were: *normothermia* (37°C), *hypothermia* (32°C for 3.75 h beginning at OGD start), and *delayed hypothermia* (32°C for 3.75 h, beginning 15 min after OGD start). Multivariate analysis of nuclear magnetic resonance metabolite quantifications included principal component analyses and the *L1-Penalized Regularized Regression* algorithm known as the *Least Absolute Shrinkage and Selection Operator* (*LASSO*).

Results—The most significant metabolite difference ($p < 0.0056$) was [2-^{13}C]glutamine's higher final/control ratio for the Hypothermia group (1.75 ± 0.12) compared to ratios for the Delayed

Address all correspondence to: Dr. Lawrence Litt, The Department of Anesthesia and Perioperative Care, 521 Parnassus Avenue, Room C455, Mail Code 0648, San Francisco, CA 94143-0648, Phone: 415-999-9202; Fax: 815-346-5193; Larry.Litt@UCSF.edu.

The authors declare no competing interests.

(1.12 ± 0.12) and Normothermia group (0.94 ± 0.06), implying a higher PC/PDH ratio for glutamine formation. *LASSO* found the most important metabolites associated with adenosine triphosphate preservation: [3,4-^{13}C]glutamate—produced *via* PDH entry, [2-^{13}C]taurine--an important osmolyte, and phosphocreatine. Final principal component analyses scores plots suggested separate cluster formation for the hypothermia group, but with insufficient data for statistical significance.

Conclusions—Starting mild hypothermia simultaneously with OGD, compared with delayed starting or no hypothermia, has higher PC throughput, suggesting that better glial integrity is one important neuroprotection mechanism of earlier hypothermia.

Introduction

Randomized clinical trials with neurological outcomes have led to mild therapeutic hypothermia (≈4°C decrease) becoming the standard of care for early treatment of hypoxic-ischemic encephalopathy from birth asphyxia.[1,2] Although it is not fully understood why a brain temperature decrease of only ≈4°C should cause dramatic outcome differences, mechanisms are known in: physiology—decreased intracranial pressure from reduced brain metabolism; biochemistry—possible activation thresholds for injurious biochemical reactions in a 4°C window; and pathology—reduction in complex processes related to *delayed neuron cell death* after oxygen restoration.

Nuclear magnetic resonance spectroscopy, (NMR) allows identification of an organism's total set of metabolites, the *metabolome*, whose group properties are studied with *metabolomics*, the science of quantifying and understanding dynamic metabolome responses to physiological changes. Because all chemical reactions are temperature dependent, it is reasonable to ask if temperature changes of 4°C produce detectable early post-asphyxia differences in specific brain metabolites or in metabolomic data sets. If post-asphyxia differences are detectable, they might help assess tissue viability, predict subsequent neurologic outcomes, and potentially suggest magnetic resonance spectroscopy approaches to individualizing patient management. This ^{13}C NMR investigation is a follow-up to our earlier ^{1}H NMR metabolomics study with the same neonatal brain slices model, in which asphyxia was also simulated by oxygen-glucose-deprivation (OGD). That previous study, which examined differences in ^{1}H metabolite patterns,[3] could not study neuron-glia metabolic differences in injury and recovery, because such requires the administration of ^{13}C-labeled substrates that exploit neuron-glia enzyme and pathway differences.

In this and the previous study *ex vivo* brain slices from 7-day-old (P7) rats underwent 45-min OGD protocols approximating the *in vivo* Vannucci-Rice asphyxia model.[4–6] Slices in three groups, treated identically until the beginning of OGD, were treated after OGD with different temperature protocols. One group was always normothermic (37°C), a second group had 3.75 h of mild hypothermia (32°C) begin with OGD, and a third group had 3.75 h of mild hypothermia begin after a 15-min delay. Multivariate analyses of extracted brain metabolite changes were quantified with high resolution NMR spectroscopy. Exploring neuron-glia differences was done by administering an equimolar mixture of two differently labeled substrates, [1-^{13}C]glucose and [1,2-^{13}C]acetate, using an experimental design well developed by others.[7–13] Because acetate is metabolized almost exclusively by astrocytes,[14–16]^{13}C NMR made it possible in the current study to compare treatment-related changes in glial and neuronal nutrient consumption, and in TCA (tricarboxylic acid) Cycle entry *via* pyruvate dehydrogenase (EC 1.2.4.1) compared to *via* pyruvate carboxylase (EC 6.4.1.1), which exists primarily in glia. Because ^{1}H NMR was performed at 21.1 Tesla (900 MHz), separate resonance peaks could be identified ^{1}H spectra for adenosine triphosphate (ATP), adenosine diphosphate, and Phosphocreatine (PCr). The hypotheses tested in this study are: 1) that different hypothermia protocols lead to statistically significant differences

in the results of principal component analyses (PCA) and projection to least squares discriminant analyses (PLS-DA), where it is assumed that metabolites are coregulated by interdependent phenomena; and, 2) that key metabolites (biomarkers) can be identified in a univariate analysis, *i.e.* one that focuses on individual metabolites and assumes that they are independent, with a *regularized regression* approach known as *L1 Penalized lasso (**l**east **a**bsolute **s**election and **s**hrinkage **o**peration).*

Materials and Methods

Cerebrocortical slice preparation and Superfusion with [1-^{13}C]glucose and [1,2-^{13}C]acetate

All animal experiments were approved by University of California, San Francisco's Institutional Animal Care and Use Committee. Three groups of experiments had protocols that were identical except for temperatures after OGD. Details of the brain slice preparation were described previously.[17–19] Briefly, in each experiment 20 cerebrocortical slices (350 μm thickness) were obtained from 10 isoflurane-anesthetized 7-day-old Sprague-Dawley rat litter-mates of either sex, and then immediately placed in a superfusion chamber containing fresh, oxygenated artificial cerebrospinal fluid (oxy-ACSF, 3 mL/min flow) whose nutrient was 10 mM glucose. At 1 h before beginning OGD, 10 mM glucose in oxy-ACSF was replaced with 5 mM [1-^{13}C]glucose and 5 mM [1,2-^{13}C]acetate, which continued during OGD and thereafter for 6 h. The superfusion chamber was partially submerged in a water bath having a combined circulator-temperature control that maintained temperatures at either 37°C (normothermic) or 32°C (hypothermic). Other details are the same as in previous studies.

Simultaneous administration of [1-^{13}C]glucose and [1,2-^{13}C]acetate[7] was used to assess different changes in neuronal and astrocytic TCA cycle activity, using the conceptual model of glutamate/glutamine recycling shown in figure 1A.[13,20] In this approach synaptic glutamate (glu) is taken up by astrocytes and converted to glutamine (gln) by glutamine synthetase (EC 6.3.1.2), an enzyme not in neurons, and then returned to neurons for glutamate restoration. ^{13}C label changes in glutamate are related to ^{13}C label changes in α-ketoglutarate that are produced in the TCA Cycle. Figure 1A suggests an assumption of many earlier studies, that ^{13}C-glutamate is in rapid equilibrium with its ^{13}C- α-ketoglutarate counterpart, with equal changes occurring in each's ^{13}C enrichment. Such has been found to be approximately true for the brain, but not be exactly true.[21,22] In this paper we assume that in each of the groups the approximation is the same and unchanged during the experiments.

Because, as outlined in figures 1B and 1C, neurons and astrocytes have different enzymes and roles in neurotransmitter recycling, and also because of rapid transfer of ^{13}C labels from α-ketoglutarate to glutamate, and from oxaloacetate to aspartate, it is possible to use downstream ^{13}C isotopomer concentrations for the computation of changes in the ratio of acetate/glucose metabolism, and changes in the ratio of flux into the TCA cycle through pyruvate carboxylase relative to flux through pyruvate dehydrogenase.

Three superfusion experiments were performed for each of the following three groups: **1) Normothermia (Group N),** in which a 37°C temperature was maintained during OGD and a subsequent 6-h recovery period; **2) Hypothermia (Group H),** which had a 3.75-h period of hypothermia (32°C) that began immediately prior to OGD with a rapid temperature decrease from 37°C. Hypothermia continued throughout OGD and afterwards throughout 3 h of recovery with oxy-ACSF. Following hypothermia, 1 h of slow rewarming to 37°C was achieved by increasing the bath temperature 1°C every 12 min. Superfusion with oxy-ACSF continued at 37°C for the experiment's last 2 h; **3) 15 min Delayed Hypothermia (Group D),** which also underwent 3.75 h of sudden hypothermia (32°C), a subsequent 1-h rewarming period, and then a 2-h recovery period. However, in this group, Group D, the

temperature decrease was delayed until 15 min after the start of OGD. In each experiment five slices for NMR spectroscopy were removed, washed, and immediately frozen in liquid nitrogen at each of four predetermined sampling times: before the onset of OGD (T_0), at the end of OGD (T_1), at the end of hypothermia (T_2), and at the end of the experiment (T_3).

At later times the five slices removed at each time point collectively underwent perchloric acid extraction of small, soluble molecules into D_2O in NMR tubes, which then underwent NMR spectroscopy for quantifications of 35 ^{1}H metabolite peaks and 23 ^{13}C metabolite peaks. Four additional frozen slices were used for non-NMR assays of ATP and glial fibrillary acidic protein (GFAP) staining, the chief outcome variables. Metabolomic assays of $^{1}H/^{13}C$ metabolite ensembles for the different sampling times were processed for associations between treatment groups and metabolomics signatures. ^{13}C data was used to look for changes in neuron-astrocyte in nutrient consumption, and for changes in TCA Cycle entry via pyruvate dehydrogenase and pyruvate carboxylase. (See Supplemental Digital Content 1, for details of OGD, perchloric acid extraction, the ATP bioassay, and GFAP staining.)

NMR data acquisition and analysis

NMR data were obtained at the Central California 900 MHz NMR Facility, which operates with National Institutes of Health support (GM68933) in QB3 facilities at University of California-Berkeley. A 21.1 Tesla Bruker Avance II NMR spectrometer (Bruker Corporation, Billerica, MA) with a 5 mm CPTXI multinuclear cryoprobe optimized for ^{13}C was used to acquire 1D ^{13}C spectra at 226.2 MHz, 1D ^{1}H spectra at 900 MHz, and *Two-Dimensional (2D) ^{1}H J-resolved NMR* spectra from which one dimensional (1D) projections were obtained along the ^{1}H axis (1D ^{1}H pJRES spectra). NMR metabolite resonances corresponding to different chemical shifts were identified and preprocessed with Bruker software (TopSpin 3.1 and AMIX), quantified with iNMR® (Nucleomatica, Molfetta, Italy), corrected for relaxation, and normalized to both the weight of the dry powder and the total spectral area. For additional details regarding NMR acquisitions and metabolite quantifications, especially that of ATP from the ^{1}H resonance on adenine's imidazole ring, see Supplemental Digital Content 1, which contains information regarding NMR Methods.

For each ^{13}C molecular position high spectral resolution, typically 0.002 ppm, permitted the identification of different ^{13}C *isotopomers*, *i.e.*, molecules where each carbon can be either ^{12}C or ^{13}C. The term is formed from the words ***isotope*** and ***isomer***. Isotopomers for a particular carbon position appear as satellite peaks that are typically 0.030 or more ppm on both sides of the central peak, *i.e*., the peak present when there is only one ^{13}C contributing to the signal. Figure 2 shows representative ^{13}C NMR peaks and isotopomers detected in our system for glutamate, glutamine, and γ-aminobutyric acid. The reference NMR signal was the upfield resonance from natural abundance ^{13}C in DSS (4,4-dimethyl-4-silapentane-1-sulfonic acid). No other natural abundance ^{13}C signals were large enough to be seen.

Calculations: (pyruvate carboxylase [PC])/(pyruvate dehydrogenase [PDH]) and (acetate/glucose)

Pathway flux ratio calculations come from ^{13}C position changes during migration through the TCA Cycle, as depicted in figures 1B and 1C, along with noting that two adjacent ^{13}C atoms can stay together during the migration, as in [1,2-^{13}C]acetate's metabolism to glutamate and glutamine.

The PC/PDH ratio for glutamate and glutamine production was estimated as (C2 − C3)/C4, and for γ-aminobutyric acid production as (C4 − C3)/C2, formulae established and used in previous studies. Similarly, for both glutamate and glutamine production the ratio of

acetate's contribution to glucose's contribution was estimated as C45/C4. In these equations numbers represent singlet resonance peaks alone (*i.e.*, exclusive of other isotopomers). Further details of the calculation involving ^{13}C metabolites are in Supplemental Digital Content 1, which contains all supplemental information regarding NMR Methods.

Statistical and Metabolomic Analyses

For both ^{1}H and ^{13}C data, metabolite quantifications for times T_1, T_2, and T_3 were normalized to initial (control) T_0 values. Within each of the T_1, T_2, and T_3 data sets three paired *t*-tests were done for each metabolite: Normothermia *versus* Hypothermia, and Hypothermia *versus* Delayed, Normothermia *versus* Delayed. To have the false positive error rate (α) be less than 5%, significance for each of the nine *t*-tests was defined by *p* values at or below a Bonferroni-corrected value, $\alpha/9$, or 0.0056.

Quantifications of identified metabolites were processed with commercial multivariate software (SIMCA P+ v.11 from Umetrics, Inc., San Jose, CA) in which quantifications for each metabolite are expressed in standard deviation units that vary equally on either side of zero. The new data set for each spectrum is then represented by a single point in a multivariate space whose dimensionality is the number of metabolites. Thereafter PCA and a partial PLS-DA are done to look for separate clustering in two dimensional (2D) planes defined by principal component Axes. For each time point there are nine points available for a 2D principal component plot, these being the three repeat spectra for each treatment group. In PLS-DA computations the integer added as a variable representing group identification introduces a bias towards group clustering.[23]

In addition to comparing ensembles of quantified ^{13}C metabolites, the chemometric feature of Bruker program AMIX 3.1 was used to check for whole spectra differences in the ^{13}C range 5 to 190 ppm. Different sized "bucket" ppm intervals were defined and centered on each metabolite's peak, except that no buckets were created for glucose and acetate, substrates present in the superfusate. Bucket sizes for each ^{13}C position included isotopomers. Intensities for each bucket were treated as independent X variables. A total of 23 X variables was used for a PCA analyses to compare nine spectra. For ^{1}H data, the spectral range from 0.50 ppm to 9.0 ppm was divided into "buckets" 0.05 ppm wide, with exclusion of the intervals 3.17 ppm to 4.0 ppm and 4.5 ppm to 5.0 ppm. A PCA analyses was also performed to compare 9 ^{1}H spectra.

Metabolite quantifications were also analyzed using a methodology known as *L1 penalized multiple linear regression* with a "*lasso*" (***l****east* ***a****bsolute* ***s****election and* ***s****hrinkage* ***o****perator*).[24] In this approach linear regression models are determined that fit an outcome variable, in this case was chosen to be the ATP value found in the luciferin bioluminescence assay done for each NMR tube. This approach, used by us and described previously,[25] is known to be well suited for situations where the number of covariates (metabolites) is large compared with the number of observations. Reviewing briefly, the *lasso* is a *regularized regression*, meaning that the function being minimized also includes a penalty term, in this case L1, the sum of the absolute values of a regression model's deviations. The L1 penalty term is weighted by a nonnegative tuning parameter λ that multiplies it. When λ is 0, the penalty function does not contribute. When λ is sufficiently large the penalty term dominates and all the coefficients are forced to zero. The analyses was conducted using the glmnet package[26] within the R Statistics language.[27] Analysis results are shown as plots of (i) cross-validated mean-squared-error *versus* λ (equivalently, the number of metabolites with nonzero coefficients) and (ii) metabolite regression coefficients *versus* the L1 penalty term. From the former one learns appropriate model sizes (number of included metabolites). From the latter one identifies the corresponding metabolites and sees the extent of their respective contributions as the model size changes.

Results

^{13}C and ^{1}H metabolite comparisons at the end of recovery for different treatment groups

Table 1 gives the results of pairwise *t*-testing for the ratios of ^{13}C metabolite quantifications at the last time point (T_3) relative to the initial time point (T_0). All values are given as mean ± SE. The Bonferroni-corrected upper limit for *p* was 0.0056 for having 5% as the upper limit for Type I errors. The most significant metabolite difference was therefore [2-^{13}C]glutamine's higher final/control ratio for the Hypothermia group (1.75 ± 0.12) compared to ratios for the Delayed (1.12 ± 0.12) and Normothermia group (0.94 ± 0.06), with both *p* values below the upper limit. Because of glutamine C2's role in calculating the ratio of (pyruvate carboxylate [PC] flux) to (pyruvate dehydrogenase [PDH] flux), the Hypothermia Group had the highest values of PC/PDH ratio for glutamine. Except for Glutamine C2, within all treatment groups changes relative to T_0 were the same within experimental error for glutamate C2, C3, and C4, and glutamine C3, and C4. The complete set of comparisons appears in figure 3A. Similar pairwise *t*-testing for ^{1}H data between groups had no significant differences as shown in figure 3B.

Greatly Improved ^{13}C and ^{1}H NMR spectral resolution; quantification of metabolites; JRES

Figure 2A shows a representative ^{13}C spectrum for a study's final time point. Figure 2B shows ^{13}C isotopomer details that cannot be seen easily in figure 2A. Table 2 lists the ^{13}C and ^{1}H resonances that were quantified, and their ppm assignments. Figures 4A–4C compare different ppm regions in two ^{1}H NMR 900 MHz spectra, obtained sequentially from the same NMR tube using different NMR methods, standard one-pulse and pJRES, but without changing static magnetic fields or disturbing the tube. The extract was from T_0, the initial time point. The pJRES spectrum substantially reduced ppm overlap of resonances for different metabolites. The PCr resonance in Figure 4B is totally resolved. Figure 4C shows downfield ^{1}H resonances, including separate ATP and adenosine diphosphate peaks.[28] Details of ^{1}H identification and quantification of ATP are with other NMR details in Supplemental Digital Content 1.

Ratios of (the total metabolite NMR signal intensity)/(the DSS reference's signal intensity)/(weight of dry powder for that spectrum, obtained after lyophilization) varied by less than 16% for all ^{1}H or ^{13}C spectra. As well, amounts of dry powder for all groups and time points varied by less than 13%. Together these indicate that within errors total metabolite pools were the same for all groups at all time points.

Acetate/Glucose consumption, PC/PDH, Time course of metabolite changes

Figure 5A shows ratios for PC *versus* PDH activity at the end of 6-h recovery. Figure 5B's bar graph shows ratios for the last three time points of acetate consumption relative to glucose consumption for glutamate production. Ratios relative to control ranged from 1.0 to 1.5, with the value at T_3 significantly being lowest for the Delayed hypothermia group ($p = 0.0013$). Figures 5C through 5H show no significant group or time differences in metabolite ratios relative to the initial time point (T_0), except for the increased ^{13}C fractional enrichment of lactate with time, and the Hypothermia Group's increased glutamine C2 at all time points.

PCA Scores Plots: Before and After Metabolite Identification

Figure 6A shows a SIMCA-P® PCA Scores Plot for T_1, T_2, and T_3 for all treatment groups. Each point represents a data set with 58 metabolite quantifications: all 23 ^{13}C and all 35 ^{1}H quantifications. In the upper left quadrant there is clustering of T_1 data (end of OGD, a time when the treatment history was the same for all groups). In Scores Plots "R^2" and "Q^2" are

among the statistical parameters used to assess fits for 2D plane and for the principal component axes, Principal Component 1 and Principal Component 2. R^2 for the 2D plane, the percentage of the total variance explained by the 2D plot was 0.56. Q^2, the average of variance percentages explained by in a cross validation procedure where the software scrambles data among the groups, was 0.43. The Scores Plot in Figure 6B ($R^2 = 0.48$, $Q^2 = 0.59$) was produced by a PLS-DA analysis, which has group ID's inserted as outcome variables (Y variables), a maneuver that tightens whatever clustering might be present, but does so with a bias towards pulling each group's points towards a different quadrant.

Figure 6C shows an unsupervised PCA Scores Plot generated by AMIX from the nine ^{13}C spectra for T_3. No metabolite assignments or isotopomer identifications were used in this "chemometric" analysis that compares entire spectral shapes by using as multiple variables the NMR quantifications in ppm intervals known as "buckets." The ppm intervals for glucose and acetate (used in the superfusate) were excluded from the analysis. Interestingly, the Normothermia Group's data isolated clustered separately in the upper left quadrant, while the other groups had data points in each quadrant. Figure 6D shows a similar PCA Plot for analysis of the ^{1}H data alone. As in figure 6C, the Normothermia Group's points are separated from the others.

L1 Penalized Regression with ATP Bioassay as the Outcome Variable

Figures 7A and 7B show ^{1}H and ^{13}C results of the L1 penalized *lasso* regression analyses, performed with "ATP-bioassay" as the outcome variable. Each analysis finds linear models for "ATP-bioassay" that are linear functions of NMR metabolites, with the number of metabolites in each model depending on λ, as explained in the Methods. In figures 7A and 7B values of log (λ) are indicated along the lower x-axis plots, while numbers of metabolites determined by lasso for models corresponding to λ are indicated along the upper horizontal axis. Y-axis values of plotted points provide Mean Square Errors (MSE) of models corresponding to λ. Lower MSE values indicate better predictive performance. Figure 7A indicates that good fits to ^{1}H data can be accomplished with models featuring between three and seven metabolites. Figure 7B indicates that good fits to ^{13}C data can be accomplished with models featuring between 3 and 10 metabolites. Companion plots inserted in figures 7A and 7B show coefficient trajectories as successive metabolites enter the model and relax the L1 penalty by decreasing λ, causing increases in the L1 norm (x-axis). For ^{1}H the first three metabolites that were selected--PCr, NAAG (N-acetylaspartylglutamate), and Taurine--stand out with PCr driving the predictive model. For ^{13}C the embedded coefficient trajectory plot, highlights the two dominant metabolites [3,4-^{13}C]glutamate and [2-^{13}C]taurine.

Quantification of GFAP-immunoreactivity

Figure 8 shows representative areas of immunostaining for GFAP and the results of ImageJ* (developed by Wayne Rasband, National Institutes of Health, Bethesda, MD) quantifications of GFAP immunoreactivity at initial and final times for the normothermia and hypothermia groups. For the Normothermia Group the observed four-fold increase in GFAP reactivity was statistically significant ($p < 0.0001$), but no increase was seen in the Hypothermia Group.

Discussion

The most important finding in this ^{13}C NMR study relates to the increase of glutamine C2 (*i.e.*, [2-^{13}C]glutamine) being highest in the Hypothermia Group at the end of recovery.

*available at http://rsb.info.nih.gov/ij. Last date accessed 5/15/13

Increased glutamine C2 was also responsible for the glutamine PC/PDH ratio calculation, (C2−C3)/C4, being higher by a factor of 2 (fig. 5A) for the Hypothermia Group. The reason for a C3 subtraction in the numerator comes from increases in glutamine C2 that occur without any flux through pyruvate carboxylase. Glutamine C2 is synthesized from [1-^{13}C]glucose by astrocytic PC after the first turn of the TCA cycle. However, the PDH pathway in figure 1B shows that if glutamate C4's precursor, [4-^{13}C] α-ketoglutarate, stays in the TCA Cycle for a second turn, it begins the second turn as oxaloacetate, with ^{13}C being equally at either C2 or C3. This increases the C2 of glutamate and glutamine, but always with equal increases in C3. Within experimental errors and independent of rate constants and relaxation times, for all groups increases from control were the same for glutamine C3, and glutamate C2, C3, and C4. The only treatment-related difference was the larger increase in the Hypothermia group's glutamine C2. Our finding is consistent with a study that found large decreases in PC flux when oxygen deprivation is severe.[29] As well it suggests that better preservation of astrocyte metabolism might be a marker or even a cause of immediate hypothermia's treatment advantage, and also possibly the mechanism for our earlier study's finding from ELISA cell death assays that showed better protection from immediate hypothermia, also by a factor of two.[19]

The glial cell emphasis in our findings fits in with the current growing emphasis in neuroresearch of astrocyte metabolism's importance to central nervous system neuronal signaling during physiological and pathophysiological states--including general anesthesia.[30–34] Historically astrocytes have been seen primarily as providers of metabolic support for adjacent neurons and regulators of local extracellular environments. However, it is now appreciated that astrocytes control numerous synaptic functions, that they have metabotropic receptors, secrete neurotransmitters, and participate in the coregulation of interdependent neuron signaling, and that they are affected by ischemia and involved in responses. It is possible that more extensive astrocyte research will produce knowledge essential for a mechanistic understanding of mild therapeutic hypothermia.

The increased glutamine and reduced GFAP staining at T_3 in the Hypothermia Group (fig. 8) is also consistent with experimental findings that GFAP expression in astrocytes correlates inversely with the activity of glutamine synthase, a neuroprotective enzyme that produces glutamine by combining glutamate with ammonia. Decreased glutamine levels in brain tissue were found to be associated with increased GFAP expression after insults,[35] which was the case for the Normothermia Group. Much of the increased GFAP expression described in the literature, occurs days and/or weeks after hypoxic or ischemic injury. However, early GFAP increases have been found starting at 4 h after an *in vivo* insult to P7 rats[36] and an *in vitro* insult to neuronal-glial embryo cells,[37] and being substantial at 12 h,[38] and 1 day.[39] Of greater relevance, however, is the recent finding in human neonates with hypoxic-ischemic encephalopathy that serum GFAP levels were increased during the first week of life, including during the first 6 h, and were predictive of brain injury on Magnetic Resonance Imaging.[40]

Another significant finding was the success of the L1-Penalized Regression algorithm in using the bioassay quantification of ATP to find important NMR biomarkers. The metabolites found by the algorithm are mechanistically significant as well, with PCr being one indicator of available phosphorylation capacity, taurine being associated with osmotic issues in brain edema, and glutamate production being a marker for the health of TCA Cycle turnover. It is not practical to have very large in N in preclinical animal studies where each point in a multivariate data set can cost thousands of dollars. The L1 Penalty algorithm is well suited for situations with smaller N, as evidenced by the very recognizable minima in the mean-squared error plots of figures 7A and 7B provide clear general examples of this algorithms' important features. As noted in review papers[41,42] the *lasso* approach has been

very widely used, is becoming more popular, and has recently been generalized from "traditional lasso", our usage, to "group lasso", a usage for higher dimensional multivariate data.

The figure 6A PCA Scores Plot provided some methodological comfort, because the analysis, which included all time points, clearly bunched together all T_1 data, which was for slices taken at the end of OGD, a time when there were no treatment differences among the groups. The T_3 Scores Plots are remarkable for not having enough data to support PCA and PLS-DA distinctions. R^2 and Q^2 values were respectable relative to the usual cut-off value for significance, 0.50. However, in the PLS-DA analysis similar Scores Plots were generated by permutation testing that had group labels scrambled randomly among all data points. Nevertheless the R^2 values provided tantalizing thoughts of possible clustering that might occur in larger data sets. The AMIX chemometric PCA Scores Plot for T_3, which uses ppm bins as variables, had the Normothermia Group's data clustered and separated from data for the other two groups (fig. 6C). It might be possible to improve the AMIX results by introducing more sophisticated preprocessing with better pH corrections or logarithmic scaling,[43] or other methods.[44–46] However, such would not circumvent the need for many more spectral data sets.

It is natural to ask how the ^{1}H results in this paper compare with ^{1}H results in our earlier study of 2010. For many ^{1}H metabolites it is not possible to make such comparisons, because for every ^{13}C metabolite signal listed in table 2, satellite NMR peaks appear in ^{1}H spectra, often overlapping with neighboring signals, causing quantifications different from those obtained when all carbon nuclei are ^{12}C. ^{1}H nuclei near a ^{13}C nucleus can sense the latter's dipole magnetic field, which causes mirror image satellite NMR peaks on either side of the unperturbed ^{1}H peak. This can be seen easily for lactate and alanine in figure 4A. As well, nutrients in this study included acetate, thereby putting heavier emphasis on glial metabolism. Although comparisons with earlier ^{1}H quantifications were not possible, ^{1}H quantifications were useful in assessing spectral differences among the treatment groups, in a way similar to *chemometric analyses* of spectra, which analyze quantifications of spectral regions without knowledge of metabolite identities contributing in those regions. The AMIX PCA (fig. 6D) plot for the ^{1}H data that coexisted with the ^{13}C data provided a confirmation of the ^{13}C AMIX Scores Plot (fig. 6C). In both plots all three points of the Normothermia Group were separated from the other groups' data points.

Our range for acetate-glucose ratios is comparable that found for rat cortex in a study of middle cerebral artery occlusion, using the same ^{13}C acetate-glucose substrates.[9] Compared to our 0.9 to 1.5 range, the acetate-glucose ratio for glutamate production in ipsilateral (ischemic) cortex was (2.32 ± 0.93) times the value for contralateral (nonischemic) cortex.[9] Changes in acetate-glucose ratios can suggest changes in metabolite traffic, such as the transfer of neuron-produced glutamate to astrocytes for conversion to glutamine, and the return glutamine to neurons for deamination to glutamate, as noted in an early study by the Bachelard group.[7]

An assumption mentioned earlier was that there is no change in the proportion of ^{13}C- α-ketoglutarate that is converted to ^{13}C-glutamate. If the kinetics of that conversion were different for the Hypothermia Group so as to increase glutamine C2, one would expect to have a similar increase in glutamate C2. Figure 5C, however, shows that levels of glutamate C2 were the same in all groups.

This study was limited to cerebrocortical tissue. However, post-OGD injury in the cerebral cortex has been found to demonstrate vulnerability similar to that of the hippocampus in a P7 rat OGD study that studied full coronal brain slice sections, and also found

pathophysiology similar to that of neonatal hypoxic-ischemic encephalopathy being suggested by various biomarkers, including tumor necrosis factor-α, lactate dehydrogenase, and inducible nitric oxide synthase.[47] We also appreciate that neuron-astrocyte metabolic interactions have more complexities than we have discussed, especially when, unlike the situation in brain slices, *in vivo* neurons use substantial aerobic metabolism to maintain the high ATP levels required by extensive neuron activation, and *in vivo* astrocytes obtain most of their ATP from glycolysis while providing neurons with substantial amounts of lactate for their energy metabolism.

In summary, we used state-of-the-art spectroscopy in a highly controlled brain slice model to test two hypotheses about finding significant metabolic differences among three different mild hypothermia protocols. We did not validate the first hypothesis, that multivariate data sets could distinguish treatment and outcome groups, due to the combined circumstances of too few data and the putative differences being much smaller than those occurring with severe hypoxia, whose data sets could be distinguished. The second hypothesis, that individual biomarkers could be identified, was strongly validated for one biomarker, glutamine produced from glucose *via* TCA Cycle entry through pyruvate carboxylase, an enzyme unique to glia. Also with regard to individual metabolites, the L1 Penalized Regression analysis (lasso), using bioassay ATP as an outcome variable, was very effective in identifying small sets of metabolites appropriate to ATP preservation. We expect that the findings and methodological advances will be useful in future investigations.

Supplementary Material

Refer to Web version on PubMed Central for supplementary material.

Acknowledgments

The work was received from the Department of Anesthesia and Perioperative Care, University of California San Francisco.

Research supported by National Institutes of Health (Bethesda, Maryland) grant #GM36747.

References

1. Roka A, Azzopardi D. Therapeutic hypothermia for neonatal hypoxic ischaemic encephalopathy. Early Hum Dev. 2010; 86:361–7. [PubMed: 20570448]
2. Wilkinson DJ, Thayyil S, Robertson NJ. Ethical and practical issues relating to the global use of therapeutic hypothermia for perinatal asphyxial encephalopathy. Arch Dis Child Fetal Neonatal Ed. 2011; 96:F75–8. [PubMed: 21068075]
3. Liu J, Litt L, Segal MR, Kelly MJ, Yoshihara HA, James TL. Outcome-related metabolomic patterns from $^{1}H/^{31}P$ NMR after mild hypothermia treatments of oxygen-glucose deprivation in a neonatal brain slice model of asphyxia. J Cereb Blood Flow Metab. 2011; 31:547–59. [PubMed: 20717124]
4. Vannucci RC, Connor JR, Mauger DT, Palmer C, Smith MB, Towfighi J, Vannucci SJ. Rat model of perinatal hypoxic-ischemic brain damage. J Neurosci Res. 1999; 55:158–63. [PubMed: 9972818]
5. Vannucci RC, Brucklacher RM, Vannucci SJ. Glycolysis and perinatal hypoxic-ischemic brain damage. Dev Neurosci. 2005; 27:185–90. [PubMed: 16046853]
6. Vannucci RC, Vannucci SJ. Perinatal hypoxic-ischemic brain damage: Evolution of an animal model. Dev Neurosci. 2005; 27:81–6. [PubMed: 16046840]
7. Taylor A, McLean M, Morris P, Bachelard H. Approaches to studies on neuronal/glial relationships by ^{13}C-MRS analysis. Dev Neurosci. 1996; 18:434–42. [PubMed: 8940616]

8. Haberg A, Qu H, Bakken IJ, Sande LM, White LR, Haraldseth O, Unsgard G, Aasly J, Sonnewald U. *In vitro* and *ex vivo* ^{13}C-NMR spectroscopy studies of pyruvate recycling in brain. Dev Neurosci. 1998; 20:389–98. [PubMed: 9778576]
9. Haberg A, Qu H, Haraldseth O, Unsgard G, Sonnewald U. *In vivo* injection of [1-^{13}C]glucose and [1,2-^{13}C]acetate combined with *ex vivo* ^{13}C nuclear magnetic resonance spectroscopy: A novel approach to the study of middle cerebral artery occlusion in the rat. J Cereb Blood Flow Metab. 1998; 18:1223–32. [PubMed: 9809511]
10. Melo TM, Nehlig A, Sonnewald U. Metabolism is normal in astrocytes in chronically epileptic rats: A ^{13}C NMR study of neuronal-glial interactions in a model of temporal lobe epilepsy. J Cereb Blood Flow Metab. 2005; 25:1254–64. [PubMed: 15902201]
11. Melo T, Bigini P, Sonnewald U, Balosso S, Cagnotto A, Barbera S, Uboldi S, Vezzani A, Mennini T. Neuronal hyperexcitability and seizures are associated with changes in glial-neuronal interactions in the hippocampus of a mouse model of epilepsy with mental retardation. J Neurochem. 2010; 115:1445–54. [PubMed: 21044073]
12. Muller B, Qu H, Garseth M, White LR, Aasly J, Sonnewald U. Amino acid neurotransmitter metabolism in neurones and glia following kainate injection in rats. Neurosci Lett. 2000; 279:169–72. [PubMed: 10688056]
13. Patel AB, de Graaf RA, Mason GF, Rothman DL, Shulman RG, Behar KL. The contribution of GABA to glutamate/glutamine cycling and energy metabolism in the rat cortex *in vivo*. Proc Natl Acad Sci U S A. 2005; 102:5588–93. [PubMed: 15809416]
14. Van den Berg, CJ. A model of compartmentation in mouse brain based on glucose and acetate metabolism. In: Balázs, R.; Cremer, JE., editors. Metabolic Compartmentation in the Brain. Macmillan; London: 1973. p. 137-66.
15. Sonnewald U, Westergaard N, Krane J, Unsgard G, Petersen SB, Schousboe A. First direct demonstration of preferential release of citrate from astrocytes using [^{13}C]NMR spectroscopy of cultured neurons and astrocytes. Neurosci Lett. 1991; 128:235–9. [PubMed: 1945042]
16. Hassel B, Bachelard H, Jones P, Fonnum F, Sonnewald U. Trafficking of amino acids between neurons and glia *in vivo* Effects of inhibition of glial metabolism by fluoroacetate. J Cereb Blood Flow Metab. 1997; 17:1230–8. [PubMed: 9390655]
17. Espanol MT, Litt L, Yang GY, Chang LH, Chan PH, James TL, Weinstein PR. Tolerance of low intracellular pH during hypercapnia by rat cortical brain slices: A ^{31}P/^{1}H NMR study. J Neurochem. 1992; 59:1820–8. [PubMed: 1402924]
18. Liu J, Hirai K, Litt L. Fructose-1,6-bisphosphate does not preserve ATP in hypoxic-ischemic neonatal cerebrocortical slices. Brain Res. 2008; 1238:230–8. [PubMed: 18725216]
19. Liu J, Segal M, Yoo S, Yang GY, Kelly M, James TL, Litt L. Antioxidant effect of ethyl pyruvate in respiring neonatal cerebrocortical slices after H_2O_2 stress. Neurochem Int. 2009; 54:106–10. [PubMed: 19041675]
20. McKenna, MC.; Dienel, GA.; Sonnewald, U.; Waagepetersen, HS.; Schousboe, A. Energy Metabolism of the Brain, Basic Neurochemistry. 8. Brady, S.; Siegel, G.; Albers, RW.; Price, DL., editors. New York: Elsevier; 2012. p. 221
21. Mason GF, Rothman DL, Behar KL, Shulman RG. NMR determination of the TCA cycle rate and alpha-ketoglutarate/glutamate exchange rate in rat brain. J Cereb Blood Flow Metab. 1992; 12:434–47. [PubMed: 1349022]
22. Berkich DA, Xu Y, LaNoue KF, Gruetter R, Hutson SM. Evaluation of brain mitochondrial glutamate and alpha-ketoglutarate transport under physiologic conditions. J Neurosci Res. 2005; 79:106–13. [PubMed: 15558751]
23. Westerhuis JA, Hoefsloot HCJ, Smit S, Vis DJ, Smilde AK, van Velzen EJJ, van Duijnhoven JPM, van Dorsten FA. Assessment of PLSDA cross validation. Metabolomics. 2008; 4:81–9.
24. Efron B, Hastie T, Johnstone I, Tibshirani R. Least angle regression. Ann Stat. 2004; 32:407–99.
25. Tibshirani R. Regression shrinkage and selection *via* the lasso. J R Stat Soc Series B Stat Methodol. 1996; 58:267–88.
26. Friedman J, Hastie T, Tibshirani R. Regularization paths for generalized linear models *via* coordinate descent. J Stat Softw. 2010; 33:1–22. [PubMed: 20808728]

27. R, Development, Core, Team: R. A language and environment for statistical computing, Reference Index Version 2.2.1 edition. Vienna, Austria: R Foundation for Statistical Computing; 2005.
28. Govindaraju V, Young K, Maudsley AA. Proton NMR chemical shifts and coupling constants for brain metabolites. NMR Biomed. 2000; 13:129–53. [PubMed: 10861994]
29. Haberg A, Qu H, Sonnewald U. Glutamate and GABA metabolism in transient and permanent middle cerebral artery occlusion in rat: Importance of astrocytes for neuronal survival. Neurochem Int. 2006; 48:531–40. [PubMed: 16504342]
30. Eroglu C, Barres BA. Regulation of synaptic connectivity by glia. Nature. 2010; 468:223–31. [PubMed: 21068831]
31. Rossi DJ, Brady JD, Mohr C. Astrocyte metabolism and signaling during brain ischemia. Nat Neurosci. 2007; 10:1377–86. [PubMed: 17965658]
32. Thrane AS, Rangroo Thrane V, Zeppenfeld D, Lou N, Xu Q, Nagelhus EA, Nedergaard M. General anesthesia selectively disrupts astrocyte calcium signaling in the awake mouse cortex. Proc Natl Acad Sci U S A. 2012; 109:18974–9. [PubMed: 23112168]
33. Franke H, Verkhratsky A, Burnstock G, Illes P. Pathophysiology of astroglial purinergic signalling. Purinergic Signal. 2012; 8:629–57. [PubMed: 22544529]
34. Attwell D, Buchan AM, Charpak S, Lauritzen M, Macvicar BA, Newman EA. Glial and neuronal control of brain blood flow. Nature. 2010; 468:232–43. [PubMed: 21068832]
35. Pekny M, Eliasson C, Siushansian R, Ding M, Dixon SJ, Pekna M, Wilson JX, Hamberger A. The impact of genetic removal of GFAP and/or vimentin on glutamine levels and transport of glucose and ascorbate in astrocytes. Neurochem Res. 1999; 24:1357–62. [PubMed: 10555775]
36. Burtrum D, Silverstein FS. Hypoxic-ischemic brain injury stimulates glial fibrillary acidic protein mRNA and protein expression in neonatal rats. Exp Neurol. 1994; 126:112–8. [PubMed: 8157121]
37. Zagami CJ, Beart PM, Wallis N, Nagley P, O'Shea RD. Oxidative and excitotoxic insults exert differential effects on spinal motoneurons and astrocytic glutamate transporters: Implications for the role of astrogliosis in amyotrophic lateral sclerosis. Glia. 2009; 57:119–35. [PubMed: 18661557]
38. Vannucci RC, Towfighi J, Vannucci SJ. Secondary energy failure after cerebral hypoxia-ischemia in the immature rat. J Cereb Blood Flow Metab. 2004; 24:1090–7. [PubMed: 15529009]
39. Ezquer ME, Valdez SR, Seltzer AM. Inflammatory responses of the substantia nigra after acute hypoxia in neonatal rats. Exp Neurol. 2006; 197:391–8. [PubMed: 16293246]
40. Ennen CS, Huisman TA, Savage WJ, Northington FJ, Jennings JM, Everett AD, Graham EM. Glial fibrillary acidic protein as a biomarker for neonatal hypoxic-ischemic encephalopathy treated with whole-body cooling. Am J Obstet Gynecol. 2011; 205:251, e1–7. [PubMed: 21784396]
41. Dasgupta A, Sun YV, Konig IR, Bailey-Wilson JE, Malley JD. Brief review of regression-based and machine learning methods in genetic epidemiology: The Genetic Analysis Workshop 17 experience. Genet Epidemiol. 2011; 35(Suppl 1):S5–11. [PubMed: 22128059]
42. Hesterberg T, Choi NH, Meier L, Fraley C. Least angle and L1 penalized regression: A review. Stat Surv. 2008; 2:61–93.
43. Parsons HM, Ludwig C, Viant MR. Line-shape analysis of J-resolved NMR spectra: application to metabolomics and quantification of intensity errors from signal processing and high signal congestion. Magn Reson Chem. 2009; 47(Suppl 1):S86–95. [PubMed: 19701928]
44. De Meyer T, Sinnaeve D, Van Gasse B, Rietzschel ER, De Buyzere ML, Langlois MR, Bekaert S, Martins JC, Van Criekinge W. Evaluation of standard and advanced preprocessing methods for the univariate analysis of blood serum ^{1}H-NMR spectra. Anal Bioanal Chem. 2010; 398:1781–90. [PubMed: 20714889]
45. Ebbels TM, Lindon JC, Coen M. Processing and modeling of nuclear magnetic resonance (NMR) metabolic profiles. Methods Mol Biol. 2011; 708:365–88. [PubMed: 21207301]
46. Zhao Q, Stoyanova R, Du S, Sajda P, Brown TR. HiRes--a tool for comprehensive assessment and interpretation of metabolomic data. Bioinformatics. 2006; 22:2562–4. [PubMed: 16895927]
47. Fernandez-Lopez D, Martinez-Orgado J, Casanova I, Bonet B, Leza JC, Lorenzo P, Moro MA, Lizasoain I. Immature rat brain slices exposed to oxygen-glucose deprivation as an *in vitro* model of neonatal hypoxic-ischemic encephalopathy. J Neurosci Methods. 2005; 145:205–12. [PubMed: 15922037]

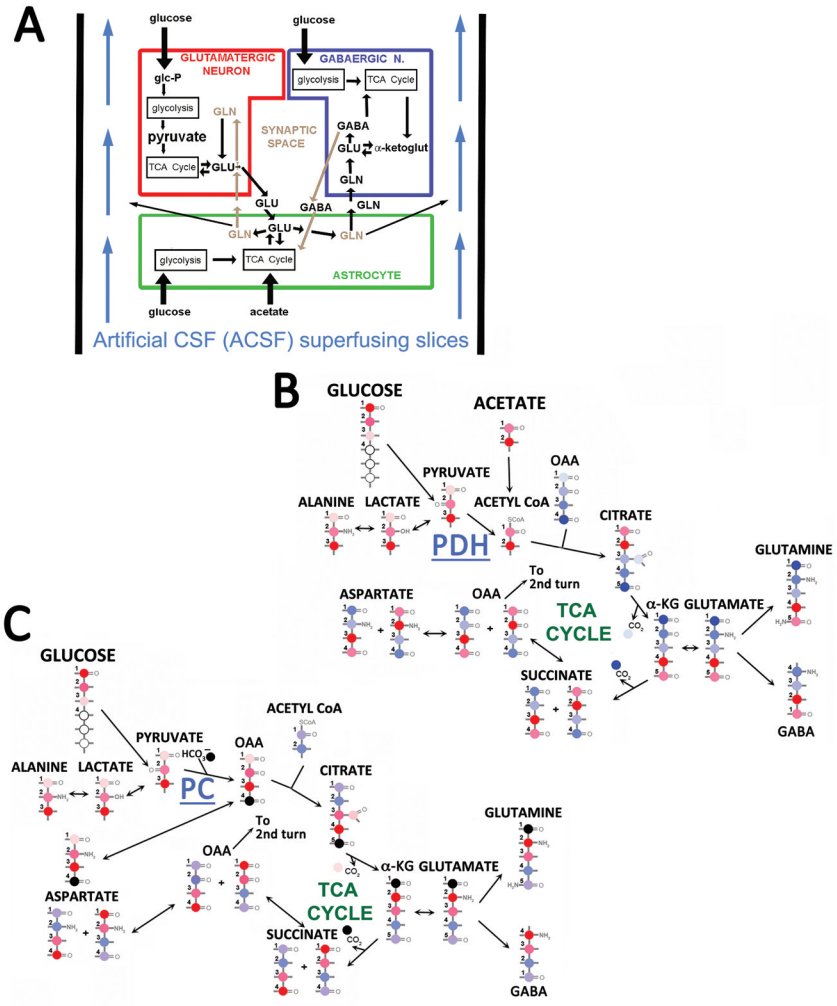

Figure 1.

(A) Schematic representation of intracellular, cellular, and synaptic metabolite traffic among astrocytes, glutamatergic neurons and GABAergic neurons. Big black arrows represent nutrient uptake: glucose alone for neurons; glucose and acetate for astrocytes. Glutamatergic neurons (red frame) release glutamate (GLU) as a neurotransmitter that is taken up from the synapse by astrocytes (green frame), converted along with astrocyte-synthesized GLU by glutamine synthase to glutamine (GLN), which is then transferred to neurons along with astrocyte-synthesized GLN. Within neurons a phosphate activated glutaminase replenishes the GLU pool. In GABAergic neurons (blue frame) GLU is converted to GABA, which is released into synapses, taken up by astrocytes, and inserted into the TCA Cycle. Small grey arrows demonstrate the efflux of glutamine from astrocytes into ACSF. Diagram is based on certain model features published elsewhere in more detail.[9,13,20] **(B and C)** ^{13}C migration patterns from ^{13}C-glucose and ^{13}C-acetate are traced through the first turn of the TCA Cycle **(B)** via pyruvate dehydrogenase (PDH) or **(C)** via pyruvate carboxylase (PC). Black circles represent ^{12}C. To find where labels are on the second turn, which begins as indicated by the arrow above the lower OAA, the reader can look at a color on the lower OAA (end of first turn), and then follow the color in the upper OAA that corresponds to the same position number. Abbreviations: GABA, γ-aminobutyric acid; TCA, tricarboxylic acid cycle; ACSF, artificial cerebrospinal fluid; OAA, oxaloacetate, α-KG, α-ketoglutarate.

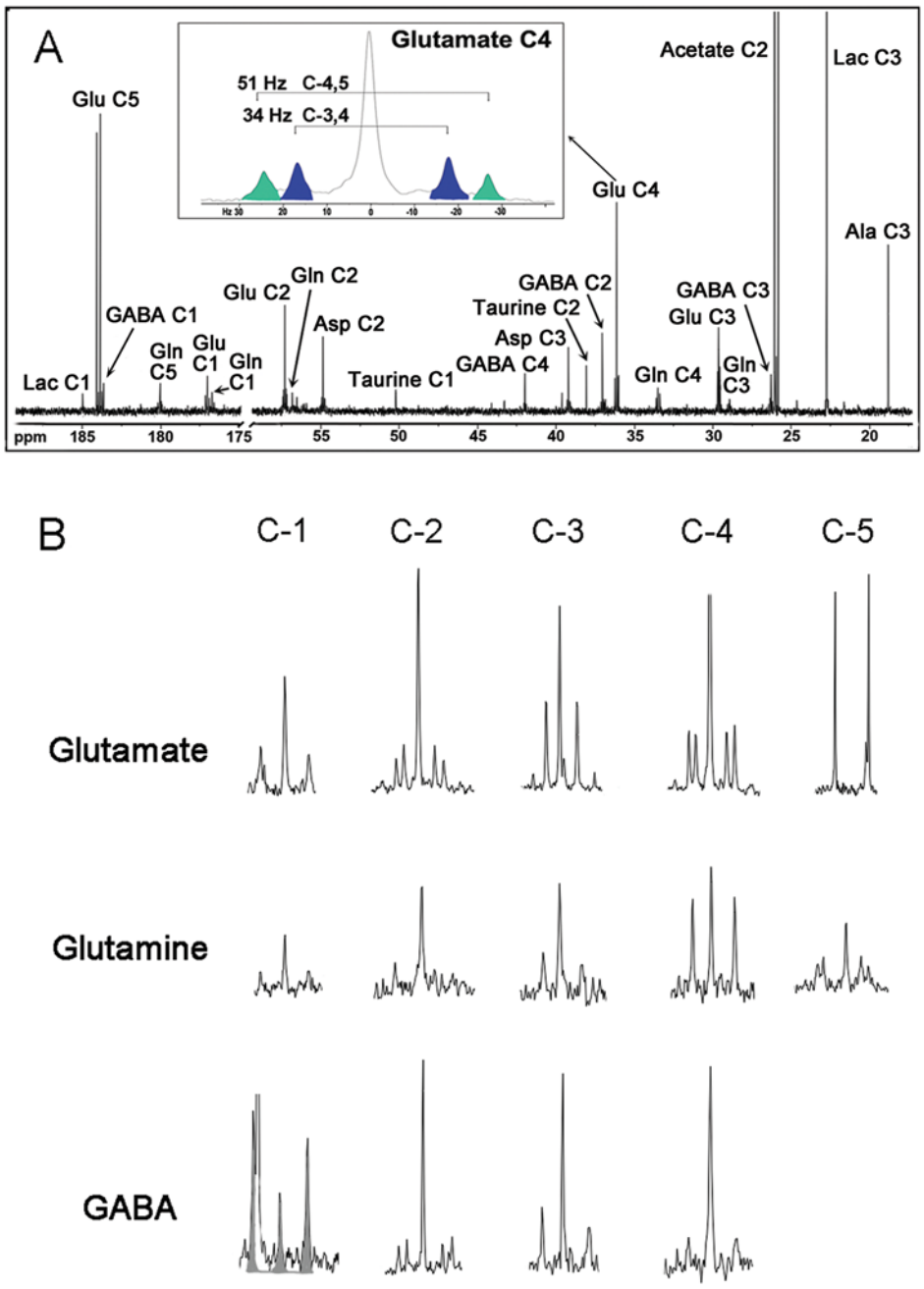

Figure 2.

(A) A representative 226 MHz ^{13}C-NMR spectrum of perchloric acid extracts from brain slices collected at the end of recovery (T_3). The range [60 – 175] ppm is omitted because it does not contain resonances quantified in this study. An expanded scale insert identifies two glutamate C4 isotopomers: [3,4-^{13}C]glu in blue and [4,5-^{13}C]glu in green, with splittings of 34 Hz and 51 Hz respectively. **(B)** Expanded ppm scale inserts of ^{13}C isotopomer patterns for glutamate, glutamine and GABA obtained from the same NMR spectrum shown in A. The vertical scales were readjusted. The resonance peaks for GABA C1 are highlighted in grey to distinguish them from the tall glutamate C5 peak that overlaps GABA C1's

downfield peak. Abbreviations: NMR, nuclear magnetic resonance; Glu, glutamate; GABA, γ-aminobutyric acid; Gln, glutamine; Ala, alanine; Asp, aspartate; Lac, lactate.

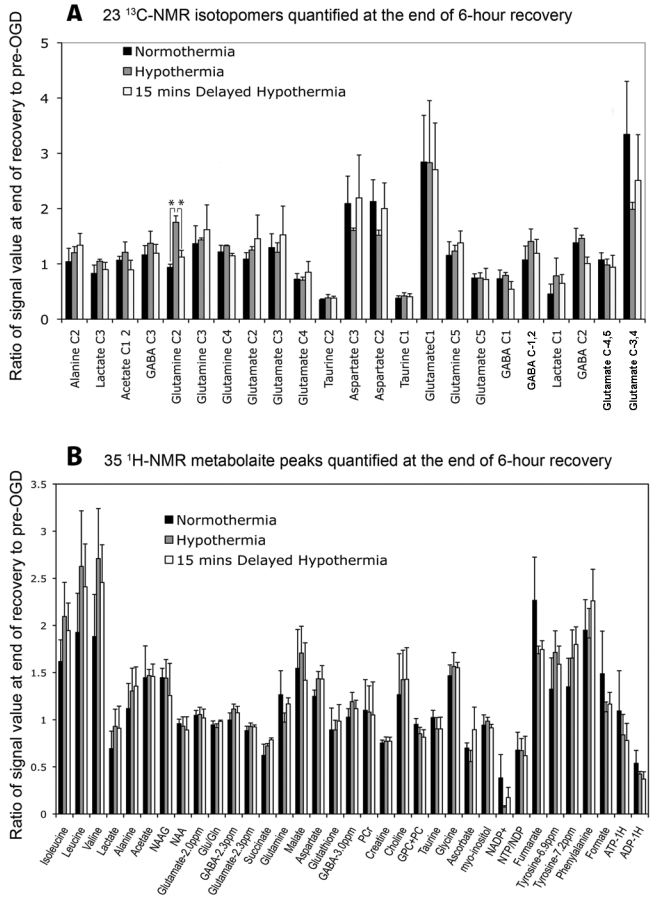

Figure 3.

^{13}C and ^{1}H NMR signal intensities at the 6-hour recovery time point (T_3) are shown relative to their initial values (T_0) for all three treatment groups prior to OGD. Vertical heights are mean ± SE (n = 3). Asterisks (*) denote statistically significant differences ($p < 0.0056$, the Bonferroni-corrected upper limit 5% for Type I errors). **(A)** Ratios for the 23 ^{13}C single peaks and isotopomers. **(B)** Ratios for the 35 ^{1}H metabolite peaks. Chemical shift suffixes are appended for the glutamate, GABA and tyrosine labels because each of these resonance peaks was quantified as an independent signal intensity. Abbreviations: OGD, oxygen-glucose deprivation; NMR, nuclear magnetic resonance; NAAG, N-acetylaspartylglutamate; NAA, N-acetylaspartate; GABA, γ-aminobutyric acid; Glu, glutamate; Gln, glutamine; PCr, phosphocreatine; GPC, glycerol 3-phosphocholine; PC, phosphocholine; ADP, adenosine diphosphate; ATP, adenosine triphosphate; $NADP^+$, nicotinamide adenine dinucleotide phosphate; NTP, nucleoside triphosphate; NDP, nucleoside diphosphate.

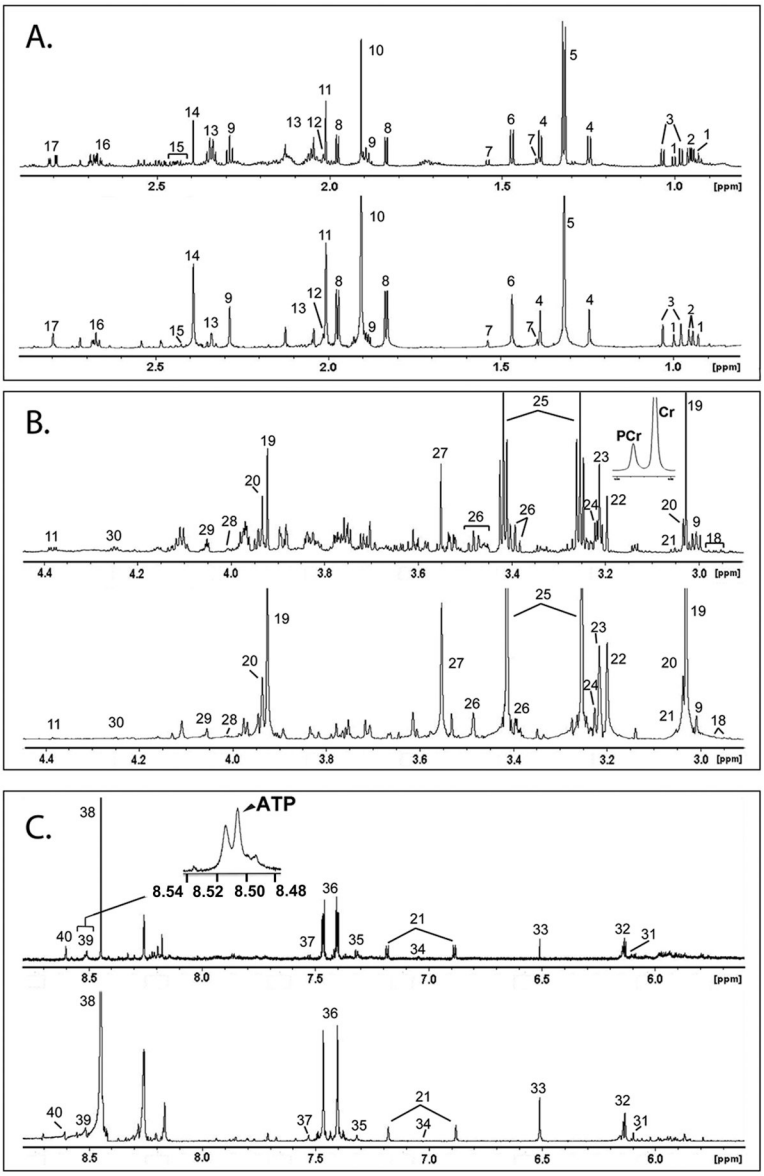

Figure 4.

(A–C) Selected segments from the 900 MHz ^{1}H-NMR spectrum for a study's initial time point (T_0). Standard one-pulse acquisition data (above) are compared with 1H NMR pJRES data for the same NMR tube (below). The disentanglement of metabolite resonances by pJRES is evident throughout, starting with the first peaks at the right margin. The text discusses two expanded inserts in **B** and **C**: the low-noise, clear separation between PCr and Cr, and the 8.51 ppm ATP resonance being encroached on its left side by another resonance peak. Spectral regions are: **(A)** 0.8 ppm– 2.9 ppm; **(B)** 2.9 ppm – 4.4 ppm; **(C)** 5.6 ppm – 8.8 ppm. ^{1}H peak assignments are: 1, isoleucine; 2, leucine; 3, valine; 4, ^{13}C-lactate; 5, lactate; 6, alanine; 7, ^{13}C-alaine; 8, ^{13}C-acetate; 9, GABA, γ-Aminobutyric acid; 10, acetate; 11, NAA, N-acetylaspartate; 12, NAAG, N-acetylaspartylglutamate; 13, glutamate; 14, succinate; 15, glutamine; 16, malate; 17, aspartate; 18, glutathione; 19, creatine; 20, PCr, phosphocreatine; 21, tyrosine; 22, choline; 23, phosphocholine; 24, glycerol 3-phosphocholine; 25, taruine; 26, glucose; 27, glycine; 28, ascorbate; 29, myo-Inositol; 30,

threonine; 31, $NADP^+$, nicotinamide adenine dinucleotide phosphate; 32, NTP/NDP, nucleoside triphosphate and nucleoside diphosphate; 33, fumarate; 34, histidine, 35, phenylalanine; 36, phthalate; 37, tryptophan; 38, formate; 39, ATP, adenosine triphosphate; 40, ADP, adenosine diphosphate.

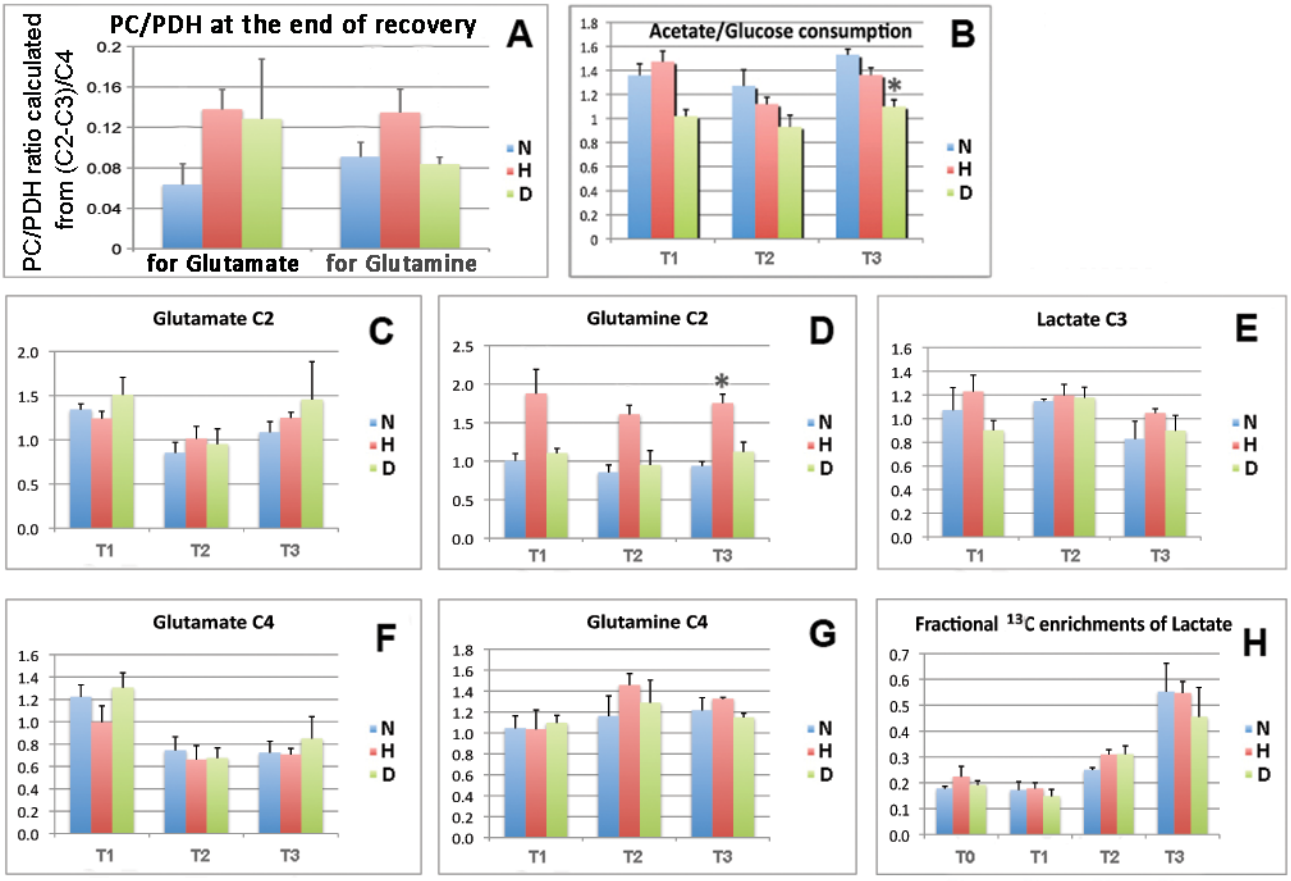

Figure 5.

Changes in neuronal-glial metabolites for all three time points and all three treatment groups: Normothermia, Hypothermia, and 15-min Delayed Hypothermia, represented by "N", "H", and "D" respectively. In graphs B through G x-axis represents time points, and y-axis represents the ratio of each time point to initial time. **(A)** Ratios for the end of recovery (T_3) of pyruvate carboxylase (PC)/(pyruvate dehydrogenase (PDH) fluxes producing ^{13}C-glutamate and ^{13}C-glutamine, calculated from (C2−C3)/C4 of glutamate or glutamine. Calculated values have no relation to control values at T_0, and are not normalized to them. In the text there is a discussion of Group H's significantly greater PC/PDH for glutamine production. **(B)** Ratios of acetate/glucose consumption glutamate production, which at the end of the recovery period was significantly decreased in Group D. Values for each time point are normalized to T_0 control data. **(C) through (G):** Metabolite quantifications for the last three time points, each measured relative to T_0 control data. **(C)** glutamate C2; **(D)** glutamine C2, which was always increased in the hypothermia group; **(E)** lactate C3; **(F)** glutamate C4, and **(G)** glutamine C4; **(H)** Fractional ^{13}C-enrichment of lactate came from ^{1}H data at 1.33 ppm, and was not normalized to control values. All data are presented as mean ± SE values for 3 experiments. Significant differences, highlighted with asterisks, are defined with $p < 0.0056$, the Bonferroni-corrected upper limit 5% for Type I errors.

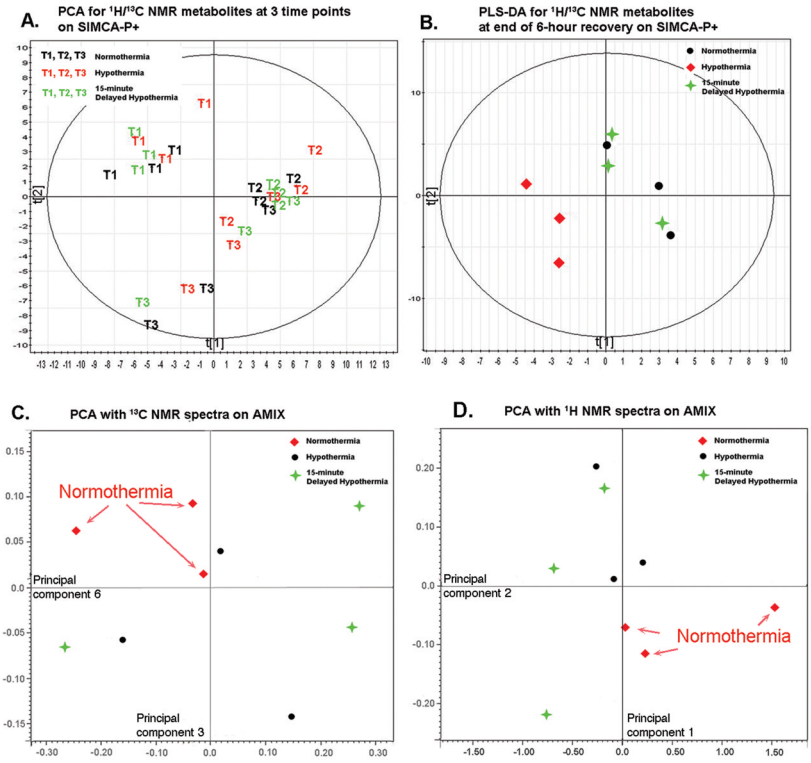

Figure 6.

(A, B) Scores Plots from multivariate analyses of $^{1}H/^{13}C$ combined data using SIMCA-P+ (Umetrics, Inc., San Jose, CA) for all 3 experimental groups: Normothermia (black), Hypothermia (red) and 15-min Delayed Hypothermia (green). Each point on the plot represents an ensemble of 35 ^{1}H and 23 ^{13}C metabolite peak quantifications measured relative to T_0 (pre-OGD) control values.(**A**) The PCA Scores Plot shows a clustering of T_1 data (end of OGD) that is separate from data for T_2 (end of hypothermia) and T_3 (end of recovery). (**B**) The PLS-DA Scores Plot shows that data at the end of recovery (T_3) for the Hypothermia group is distinct from data from the other two groups. **(C, D)** PCA Scores Plots produced by the chemometric software in Bruker's AMIX 3.1™ (Bruker Corporation, Billerica, MA) analysis of T_3 spectra for all 3 groups: Normothermia (red), Hypothermia (black) and 15-min Delayed Hypothermia (green). In **(C)** each point represents a full ^{13}C spectrum. In **(D)** each point represents a full ^{1}H spectrum. Although more data are needed for obtaining statistically significant results, the plot suggests potential separate clustering of normothermia points. Abbreviations: OGD, oxygen-glucose deprivation; NMR, nuclear magnetic resonance; PCA, principal component analysis; PLS-DA, Partial least squares Discriminant Analysis.

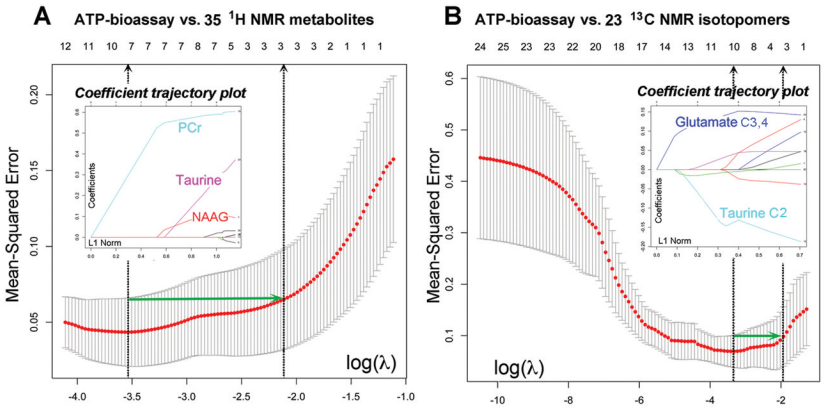

Figure 7.

(**A**) and **(B)** Results of two *L1-penalized lasso regression* analyses are shown in which ATP-bioassay was the outcome variable, and metabolite quantifications other than ATP-1H were the predictor variables. As explained in the text, the tuning parameter λ adjusts the penalty term. L1 is sum of absolute deviations. Regression function is equal to residual sum of squares (RSS) subtract L1. When λ is zero, off-scale to the left on the x-axis, the fit is an ordinary linear regression involving all metabolites. As λ increases from zero the increasing penalty decreases the number of metabolites that fit the model, as indicated along the horizontal top border. Cross-validation mean square errors (MSE) are indicated by red dots. Black dotted vertical lines bracket the range of λ, which is also the range of the number of metabolites in models that provide "good" linear fits. In (A) the X variables are the 35 ^{1}H metabolites. Models with 3–7 variables provided good fits, and PCr and unlabeled taurine were dominant. In (B) the X variables are the 23 ^{13}C metabolites, models with 3–10 variables provided good fits, and [3,4-^{13}C]glutamate and [2-^{13}C]taurine are were dominant. Abbreviations: ATP, adenosine triphosphate; PCr, phosphocreatine; NMR, nuclear magnetic resonance; NAAG, N-acetylaspartylglutamate.

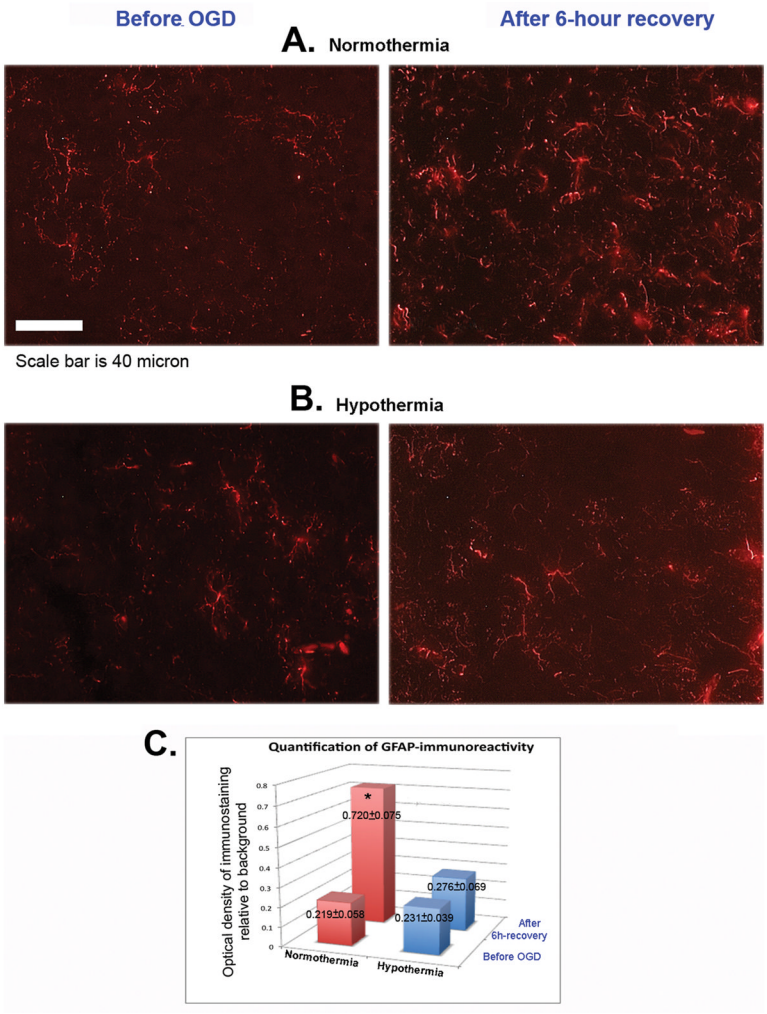

Figure 8.

GFAP staining shows immunoactivity (red) in rat brain slices treated with normothermia (A) and hypothermia (B). In (A) and (B) pictures at the left are from samples obtained before OGD insult, while pictures at the right are from samples obtained after the 6-hour recovery. (C) A 3D bar graph shows a comparison of GFAP immunoreactivity quantifications for two groups at two time points, obtained as described in the text. Values are for GFAP red fluorescent density relative to the background. Numbers at the top of each bar are given as mean ± SE (n = 3). The asterisk indicates that the normothermia group's GFAP immunoractivity at 6 hours after OGD was significantly ($p < 0.0001$) greater than in the other 3 sets. Abbreviations: GFAP, glial fibrillary acidic protein; OGD, oxygen-glucose deprivation.

Table 1

Metabolite Comparisons at the 6-hour recovery time point (T_3)

Metabolite	Values in each group (Mean ± SE)		Ratios within groups (Mean ± SE)		*P* value
Glutamine C2	H	1.75±0.12	**H÷N**	1.87±0.17	0.0014*
	D	1.12±0.12	**H÷D**	1.56±0.20	0.0049*
	N	0.94±0.06	**D÷N**	1.20±0.15	0.25
Glutamine C4	H	1.33±0.01	**H÷N**	1.09±0.11	0.46
	D	1.15±0.04	**H÷D**	1.16±0.04	0.04
	N	1.22±0.12	**D÷N**	0.94±0.10	0.64
PC/PDH for glutamine	H	0.14±0.01	**H÷N**	1.48±0.19	0.0164
	D	0.08±0.00	**H÷D**	1.61±0.17	0.0084
	N	0.09±0.01	**D÷N**	0.92±0.09	0.60
Acetate/Glucose for glutamate	H	1.36±0.06	**H÷N**	0.89±0.05	0.0695
	D	1.10±0.06	**H÷D**	1.24±0.08	0.0138
	N	1.53±0.05	**D÷N**	0.72±0.04	0.0013*

*Comparisons with $p < 0.0056$ have significant differences in the context of Bonferroni corrections and a Type I error less than 0.05.

PC, pyruvate carboxylase; PDH, pyruvate dehydrogenase.

"H": Hypothermia group; "D": Delayed hypothermia group; "N": Normothermia group.

Table 2

^{1}H and ^{13}C chemical shifts of NMR resonance peaks in Figure 2 and 4 relative to DSS Values are for central peaks of satellites (^{1}H) and isotopomers (^{13}C)

	^{1}H Metabolite	ppm		^{13}C Metabolite	ppm	isotopomers
1	Isoleucine	0.930	1	Alanine C3	18.87	
2	Leucine	0.947	2	Lactate C3	22.81	
		0.958	3			C2,3
3	Valine	0.981	4	NAA C6	24.7	
		1.033	5	Acetate C2	25.9	C1,2
4	Lactate 13C	1.247			26.12	
		1.389	6	GABA C3	26.34	
5	Lactate	1.320	7			C2,3
7	Alanine 13C	1.396	8	Glutamine C3	28.95	
		1.540	9			C2,3 or C3,4
6	Alanine	1.470	10	Glutamate C3	29.68	
8	Acetate 13C	1.835	11			C3,4
		1.976	12			C4,5
9	GABA	1.892	13	Glutamine C4	33.56	
10	Acetate	1.907	14			C4,5
11	NAA	2.010	15	Glutamate C4	36.19	
12	NAAG	2.017	16			C3,4
13	Glutamate	2.045	17			C4,5
13	Glutamate	2.127	18	Succinate C2&C3	36.9	
9	GABA	2.288	19	GABA C2	37.11	
13	Glutamate	2.341	20			C2,3
14	Succinate	2.393	21			C1,2
15	Glutamine	2.429	22	Taurine C2	38.12	
16	Malate	2.676	23	Aspartate C3	39.26	
17	Aspartate	2.800	24			C2,3
18	Glutathione	2.946	25			C3,4
		2.966	26	GABA C4	42.04	

	^{1}H Metabolite	ppm		^{13}C Metabolite	ppm	isotopomers
9	GABA	3.006	27			C3,4
19	Creatine	3.028	28	NAA C3	42.36	
20	PCr	3.034	29	Taurine C1	50.23	
21	Tyrosine	3.050	30	Aspartate C2	54.92	
22	Choline	3.196	31			C2,3
23	Pcho	3.213	32			C1,2
24	GPCho	3.223	33	NAA C2	55.96	
25	Taurine	3.250	34	Creatine C5	56.59	
		3.410	35	Glutamine C2	56.88	
26	Glucose	3.401	36			C1,2
		3.482	37	Glutamate C2	57.36	
27	Glycine	3.550	38			C2,3
17	Aspartate	3.889	39			C1,2
19	Creatine	3.922	40	Glucose C6	62.91	
20	PCr	3.934	41	Glyceryl C3	65.22	
28	Ascorbate	4.006	42	Lactate C2	71.22	
29	Myo-inositol	4.051		**--------Skip 72-175 ppm--------**		
30	Threonine	4.247	43	Glutamine C1	177	
11	NAA	4.380	44			C1,2
31	$NADP^{+}$	6.107	45	Glutamate C1	177.3	
32	NTP/NDP	6.138	46			C1,2
33	Fumarate	6.509	47	Glutamine C5	180.32	
21	Tyrosine	6.888	48			C4,5
		7.184	49	GABA C1	184.05	
34	Histidine	7.051	50			C1,2
35	Phenylalanine	7.319	51	Glutamate C5	184.15	
36	Phthalate	7.404	52		184.38	C4,5
		7.466	53	Lactate C1	185.27	
37	Tryptophan	7.528				
38	Formate	8.446				
39	ATP	8.508				

	^{1}H Metabolite	ppm	^{13}C Metabolite	ppm	isotopomers
40	ADP	8.601			

Abbreviations: NMR, nuclear magnetic resonance; DSS, 4,4-dimethyl-4-silapentane-1-sulfonic acid; GABA, γ-aminobutyric acid; NAA, N-acetylaspartate; NAAG, N-acetylaspartylglutamate; PCr, phosphocreatine; GPCho, glycerophosphocholine; $NADP^{+}$, nicotinamide adenine dinucleotide phosphate; NTP, nucleoside triphosphate; NDP, nucleoside diphosphate; ATP, adenosine triphosphate; ADP, adenosine diphosphate.